GEOLOGICA CARPATHICA, APRIL 2008, 59, 2, 89–102

Upper Jurassic–Lower Cretaceous tectonothermal events in the Southern Gemeric Permian rocks deduced from electron microprobe dating of monazite (Western Carpathians, Slovakia)

ANNA VOZÁROVÁ[1], PATRIK KONEČNÝ[2], JOZEF VOZÁR[3] and MILOŠ ŠMELKO[1]

[1]Comenius University Bratislava, Faculty of Natural Sciences, Department of Mineralogy and Petrology, Mlynská dolina, pav. G, 842 15 Bratislava, Slovak Republic; vozarova@fns.uniba.sk
[2]State Geological Institute of Dionýz Štúr, Mlynská dolina 1, 817 04 Bratislava, Slovak Republic; konecny@gssr.sk
[3]Geological Institute, Slovak Academy of Sciences, Dúbravská cesta 9, P.O. Box 106, 840 05 Bratislava, Slovak Republik; geoljovo@savba.sk

(Manuscript received January 15, 2007; accepted in revised form December 13, 2007)

Abstract: The age and chemical composition of monazite from the Permian acid metavolcanic/volcaniclastics of the Southern Gemeric Unit (from the 1st and 2nd volcanogenic horizons of the Rožňava Formation) and the Bôrka Nappe (the Bučina Formation) was studied by the microprobe chemical method. Monazites from the 2nd volcanogenic horizon of the Rožňava Formation as well as from the Bôrka Nappe occur mostly in the form of small irregular grains about 5–10 µm in size always surrounded by the metamorphic white mica-phengite. Although substantial zonality in single grains was not observed, inter-granular variation in composition is much pronounced and it is mainly attributed to the variation in ThO_2 concentration in the range from 0.9 to 14.5 wt. % (5.1 wt. % in average). Monazites from the 1st volcanogenic horizon of the Rožňava Formation are larger, ~30–40 µm in diameter, and most of them are showing concentric zonality related to the age. Rounded cores mostly of Permian age are surrounded by Alpine rims. ThO_2 concentration is more restricted up to 7.2 wt. %. The average is correspondingly lower ~3.5 wt. %. The majority of the monazites from the Permian acid metavolcanic rocks record an Alpine tectonothermal event around 148 ± 8 Ma. Alpine age data divided according to the statistical modeling present two successive sub-events yielding ages of 167 ± 12 and 136 ± 10 Ma. Jurassic event is interpreted as a strong reworking linked to the subduction/accretion processes. Obduction of the Meliata accretionary prism, and strong subduction-related fluid flow over the Southern Gemeric domain including its Permian envelope unit are presumed. The successive Early Cretaceous (136 ± 10 Ma) compression within the Inner Western Carpathians domain was followed by polyphase Alpine tectonic evolution connected with the gradual Cretaceous collision and indentation at about 100 Ma. The evidence for the Early Permian magmatic event at 276 ± 25 Ma in the 1st volcanogenic horizon of the Rožňava Formation recorded in the corroded monazite cores is presented for the first time.

Key words: Western Carpathians, Southern Gemeric Unit, monazite dating, Early Permian metavolcanites, Alpine overprint.

Introduction

During the latest Carboniferous-Early Permian times, the final phase of the Variscan orogenic extension produced series of small strike-slips and extensional continental basins across the Central and Inner Western Carpathians realm. Within these basins continental successions of Upper Pennssylvanian-Cisuralian (Stephanian to Autunian) age were deposited.

Following the end of Variscan contraction in the latest Carboniferous times, subsequent Stephanian and/or Early Permian magmatic activity and basin formation in both the internal Variscides (the area within the Central Western Carpathians) and the external Variscides (the area of the Inner Western Carpathians) took place. Within the external, the Inner Western Carpathian Zone, post-Variscan sequences are developed only in the Southern Gemeric Unit. Here, the Early Permian autochthonous continental Rožňava Formation (lower part of the Gočaltovo Group defined by Bajaník et al. 1981), is considered as a relic of the former basin filling related to the initial stage of post-Variscan rifting (Fig. 1a). The compositionally mature siliciclastic sediments are connected with the rift-related rhyolite-dacite subaerial volcanism.

The Southern Gemeric crystalline basement complex and its Permian envelope is overthrusted by the Late Paleozoic–Mesozoic Bôrka Nappe complexes of the Meliatic Unit (Fig. 1b). Within the our study area, the Bôrka Nappe Late Paleozoic sequence is represented by the Bučina Formation sequence. This is composed of a huge mass of rhyolite-dacite volcaniclastics associated with scarce volcanites (Mello et al. 1998). Lithologically is very similar to the Southern Gemeric Permian envelope unit. This was the reason why the whole Permian sequence of the Bôrka Nappe was formerly classified as the Rožňava Formation, in spite of basic differences in the tectonic position and tectonometamorphic deformation of different parts (Bajaník et al. 1984). For this reason, the main goal of our investigation was the age determination

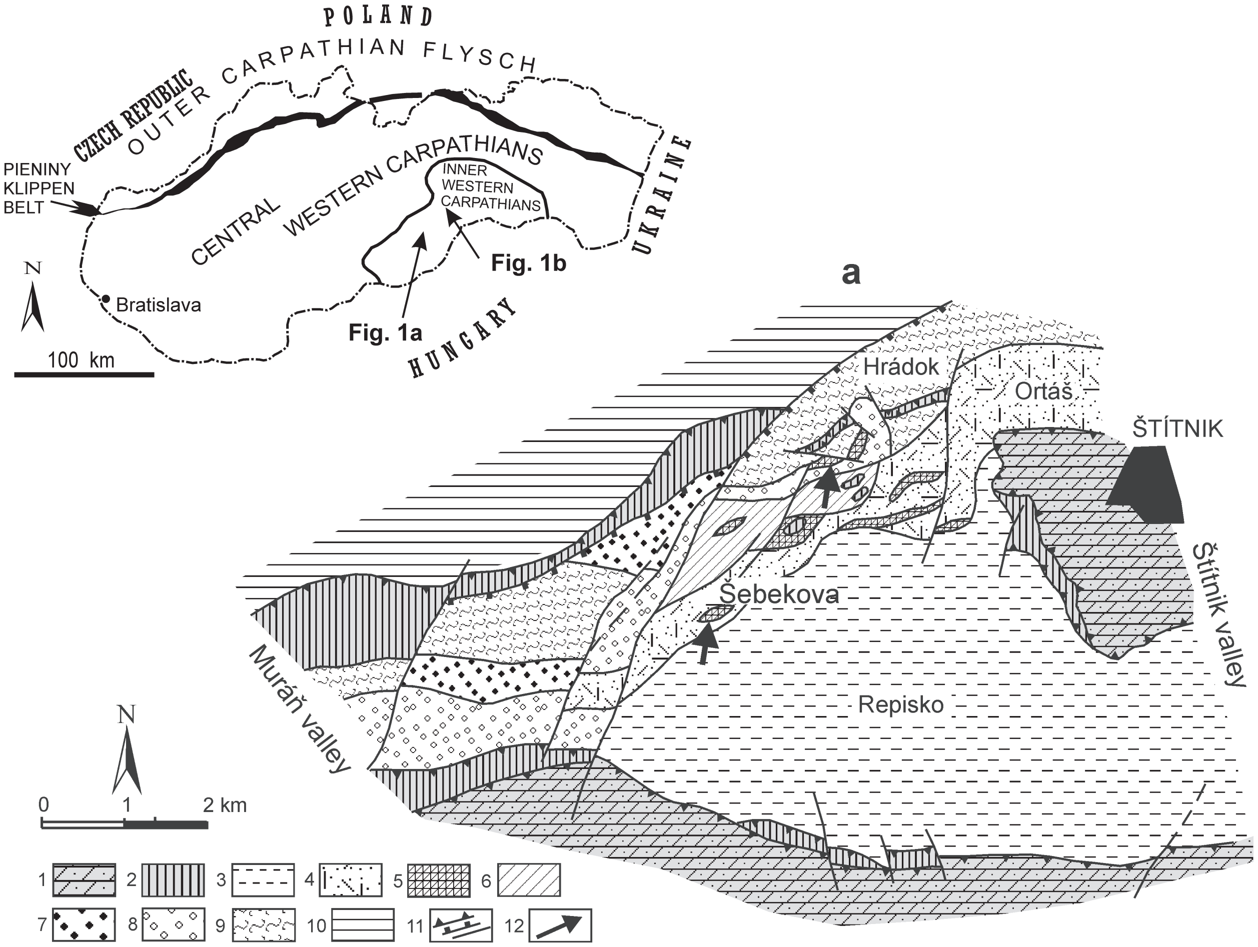

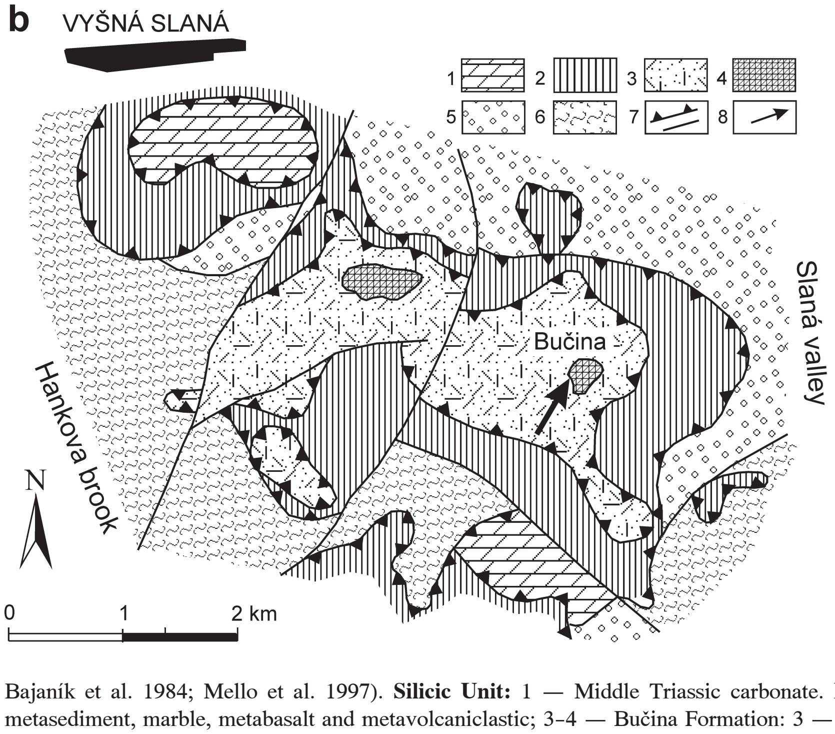

Fig. 1. **a** — Geological scheme of the Štítnik-Jelšava area with localization of samples (modified after Bajaník et al. 1984; Mello et al. 1997). Explanations: **Turnaic Unit:** 1 — Middle to Upper Triassic dolomite, limestone, cherty limestone. **Meliatic Unit:** 2 — Bôrka Nappe sequence undivided. **Southern Gemeric Unit:** 3–8 — Gočaltovo Group (Lower-Upper Permian): 3 — metasandstone, shale, scarce lenses of phosphatic sandstone, 4 — tuffaceous metasandstone and metaconglomerates, 5 — rhyolite-dacite and their volcaniclastic, 6 — medium- to coarse-grained quartzose metasandstone with local intercalation of conglomerate, 7 — massive, medium- to coarse-grained sandstone, 8 — oligomict conglomerate, 9 — Gelnica Group (Early Paleozoic) — sequence undivided, 10 — overthrust line, fault; 11 — observed localities. **b** — Geological scheme of the Bučina area with localization of sample (modified after Bajaník et al. 1984; Mello et al. 1997). **Silicic Unit:** 1 — Middle Triassic carbonate. **Meliatic Unit (*Bôrka Nappe*):** 2 — siliciclastic metasediment, marble, metabasalt and metavolcaniclastic; 3–4 — Bučina Formation: 3 — metasandstone, volcaniclastic metasandstone and conglomerate, 4 — rhyolite-dacite and their volcaniclastic; **Southern Gemeric Unit:** 5 — Gočaltovo Group (Permian): oligomictic metaconglomerate, metasandstone; 6 — Gelnica Group (Early Paleozoic): phyllite, metagraywacke, porphyroid, lydite undivided; 7 — overthrust line, thrust fault; 8 — localities.

of the acid volcanogenic horizons in the two tectonic units and the correlation of their tectonothermal history.

On condition of negligible initial common lead in monazite the total Pb measured by microprobe corresponds to the age and Th contents (Suzuki & Adachi 1991a,b, 1994; Montel et al. 1996). The monazites present in the Southern Gemeric and the Bôrka Nappe acid metavolcaniclastic rocks were used for chemical dating of the magmatic and metamorphic events.

Geological setting

The late Variscan, post-orogenic overstep sequence of the Southern Gemeric Unit (Fig. 1a) is represented only by the Permian continental and near-shore, lagoonal-sabcha sedimentary complexes. They unconformably overlapped their Lower Paleozoic basement, the volcano-sedimentary deep-water turbidites of the Gelnica Group and the Štós Formation (defined in the Variscides as the Gelnica Terrane, Vozárová & Vozár 1996). The setting of the Permian envelope sequence is identical in almost all localities. It occurs either in the tectonic underlier of the high-pressure Bôrka Nappe of the Meliatic Unit or directly below the Turnaic Unit.

The Permian volcano-sedimentary complex is generally characterized by a high content of mineral mature detritus mainly in its basal part. Conspicuous upward fining is accompanied by a relative decrease of mineralogical maturity and grain-size of sediments (Vozárová 1977). The whole sequence is subdivided into two lithostratigraphic units: the Rožňava and Štítnik Formations (Fig. 2).

The characteristic lithotype of the Rožňava Formation is the oligomictic, quartzose conglomerate, with the indistinct stratification. The whole sequence is subdivided vertically into two large cycles, starting with conglomerate horizons at the base of each and a sandstone-shale member between their two. Dominant are stream channel and sheet-flood deposits, with unimodal transport system. On the basis of microflora (Planderová 1980) the Early Permian age of the Rožňava Formation is assumed. Both conglomeratic horizons are connected with rhyolite-dacite subaerial volcanism. Their chemical composition corresponds to the calc-alkaline and alkaline magmatic type. This intra-basin acid volcanism took place within two relative short time periods, and ceased at the end of main phase of crustal extension as a response to the Variscan late-orogenic collapse. The magma ranges in composition from calc-alkaline rhyolite and rhyodacite to alkaline quartz-alkali feldspars trachyte. The emplacement of the Rožňava Formation acid volcanites was accompanied by the eruption of volcanic ashes, laterally extensive block and ash flows and their reworked epiclastic deposits. The initial stage of volcanism (1^{st} conglomeratic horizon) is associated with ignimbrites. The schematic overview of lithostratigraphic relationships is shown on Fig. 2.

The gradually prograding Štítnik Formation is a monotonous complex of cyclically alternating sandstones, siltstones and shales. Lenses of carbonatic sandstones and dolomitic limestones (calcitified dolostone, "dedolomite") with intercalations of shales occur only in its upper part. Thin lenses of phosphatic sandstones and sediments with extremely high content of albite (albitolites) are solitary. The sediments contain relatively high amounts of rhyolite/dacite detritus, presumably redeposited from the Rožňava Formation. The sedimentary environment is interpreted as alluvial-lacustrine and lacustrine, with high-alkaline and eutrophic lakes in some places, prograding into near-shore, lagoonal-sabcha facies (Vozárová & Vozár 1988; Vozárová & Rojkovič 2000). Late Permian biostratigraphic age determinations are known only from the uppermost part of the Štítnik Formation (Šuf 1963).

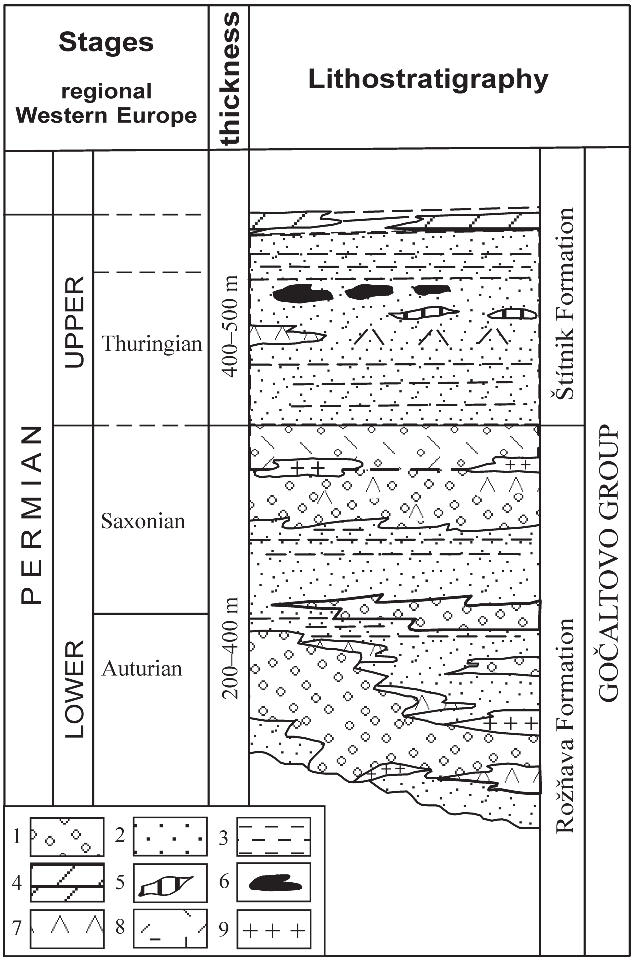

Fig. 2. Gočaltovo Group lithostratigraphic scheme: **1** — conglomerate, **2** — sandstone, **3** — shale, **4** — dolomitic limestone, **5** — albitolite, **6** — phosphatic sandstone, **7** — rhyolite–dacite pyroclastics, **8** — tuffaceous/sedimentary mixed rocks, **9** — rhyolite-dacite.

Sequences of the Southern Gemeric Permian are deformed and recrystallized, within metamorphic grade reaching P-T conditions from the anchizone to low-temperature part of the greenschist facies (Šucha & Eberl 1992; Vozárová 1996; Vozárová & Rojkovič 2000).

In the Nižná Slaná Depression (to the north of Štítnik and in the vicinity of Jelšava) numerous tectonic scales of the Upper Paleozoic and Mesozoic rock complexes of the Bôrka Nappe occur (Fig. 1b). The high-pressure Bôrka Nappe rock complex represents a relic of the accretionary prism originated as a result of the Jurassic subduction of the oceanic bottom and thinned continental margin of the Meliata Ocean (Mello et al. 1998). Their relationship to the underlying Lower and Uper Paleozoic rock complexes of the Southern Gemericum is tectonic in all sections. The part of the Bôrka Nappe tectonic scales (defined in the Jasov and Bučina Formations) consists of siliciclastic sediments associated with the huge mass of rhyolite-dacite volcaniclastics and volcanites in places (Fig. 3). The complex rich in acid volcanic material was first denoted by Fusán (1959) as the Bučina Beds and linked to the autochthonous Late Paleozoic envelope. Further investigations proved their allochthonous position on the Paleozoic rock complexes of the Southern Gemeric Unit. Later, the whole complex was redefined as the Bučina Formation and coordinated with the Bôrka Nappe (Mello et al. 1997, 1998). But likewise, a distinct lithological similarity (mature clastic detritus and petrological and geochemical equal volcanism) with the Southern Gemeric Rožňava Formation exists (Bajaník et al. 1984).

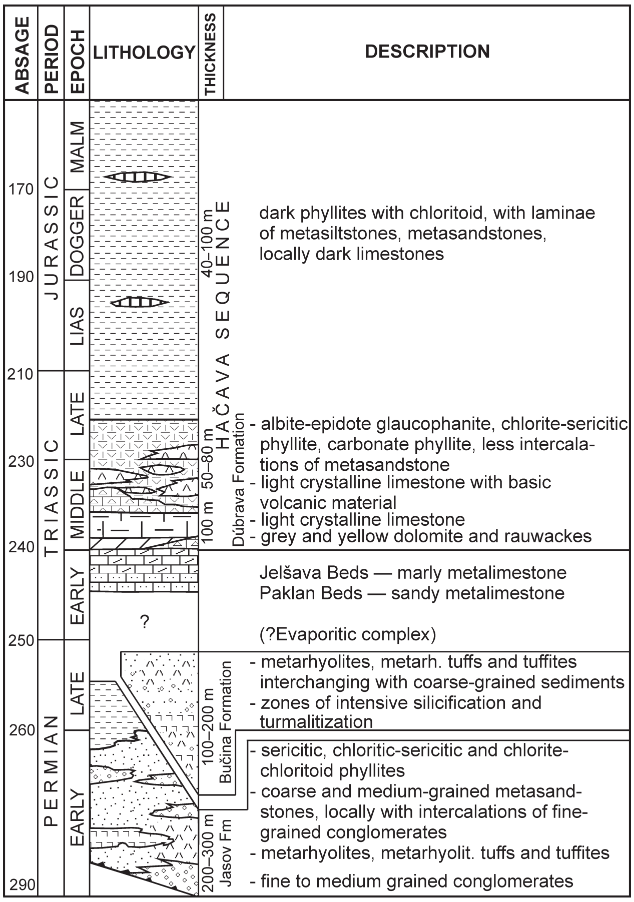

Fig. 3. Bôrka Nappe lithostratigraphic scheme based on Mello et al. (1997, 1998).

In contrast to the Rožňava Formation, the Bučina Formation with only a minor sedimentary fill contains mostly products of rhyodacitic volcanism, namely lava flows, ash beds generally of phreatomagmatic origin and ignimbrites. Sediments, such as redeposited acid volcaniclastics mixed with mineral mature quartzose detritus of conglomeratic and sandy grain size distribution are most frequent. Even though, no biostratigraphic data from sediments had been obtained, the high grade of petrological and geochemical similarity of the both volcanic formations justifies the correlation of the Bučina Formation with the Permian.

Analytical methods

The monazites were analysed using the electron microprobe Cameca SX-100 in the Department of Microanalysis at State Geological Institute of Dionýz Štúr (Slovak Geological Survey) in Bratislava. The analytical conditions suitable for the monazite dating have to meet some compromising measurement conditions to achieve sufficient counts, measuring time and the degree of contamination of the analysis place. It was used 15 kV accelerating voltage which is sufficient for REE, Th, U, Pb lines excitation. It is less harmful for contamination of the analysis place and for the ZAF correction factors that are lower in the case of 20 kV. Lead was measured 130 s, Th 35 s, U 65 s, REE 25 s and all other elements 15 s. High beam current 100 nA was used to achieve the sufficient counts for statistical counting. Natural minerals and chemical compounds were used for the calibration: Al-Al_2O_3, Si-SiO_2, P-apatite, Ca-wollastonite, REE-$(REE)PO_4$, Pb-PbS, U-UO_2 and Th-ThO_2. Th, U, Pb, Y, P were measured with LPET, REE with LLIF, As-$GaAs_2$ and Si, Al with TAP analysing crystal. X-ray Ka lines were used for Si, Al. Ma lines were used for Th, Pb and Mb line for U, La and Lb line for REE elements. The existing interferences between REE elements and $PbM\alpha_1$-$YL\gamma_1$ and $UM\beta_1$-$ThM\gamma_1$ were corrected with an empirical correction factor.

Chemical monazite analyses were recalculated to the ages using the statistical model developed by Montel et al. (1996). A program DAMON developed by P. Konečný (during 2004–2006) was used for recalculation procedure as well as age histogram and isochrone construction. More detailed information on measurement conditions and the recalculation method is given in Konečný et al. (2004).

Sample characterization

Four samples were selected for the electron microprobe dating of monazite from the Permian metavolcanic rocks of the Southern Gemericum and the Bôrka Nappe (Fig. 1a,b). Samples 1/SM and 2/SM are located in the upper conglomerate horizon of the Rožňava Formation, in the area of Šebeková Hill, south of Gočaltovo village. Both are associated with the second volcanogenic horizon of the Rožňava Formation. Sample 4/SM comes from the basal part of the Rožňava Formation (1st volcanogenic horizon). Sample 3/SM is located near the Bučina height, in the Bučina Formation, which is the main lithostratigraphic sequence of the partial tectonic scale of the Bôrka Nappe (Fig. 1b).

The Southern Gemeric Permian metavolcanites and metavolcaniclastics have a mainly felsitic and vitroclastic character. The related metavolcaniclastics contain a small amount of deformed relics of β-quartz, perthitic alkali feldspars and scarce biotite as well as abundant fragments of felsites and recrystallized volcanic glass. The volcaniclastics from the first volcanogenic horizon of the Rožňava Formation are characterized by distinct preservation of ignimbrite structure, with relics of deformed "fiamè". The newly formed metamorphic mineral assemblage is represented by the fine-grained aggregate of quartz + phengite ± chlorite ± albite. The chemical composition of the acid volcanites largely falls into rhyolite-dacite peraluminous suite. They typically contain 4.5 %–5.4 % alkalies highly dominated by K_2O and have fairly low levels of MgO, CaO and FeO_t. The Rožňava Formation volcanites are generally markedly enriched in B, Zr and Rb and only slightly enriched in La and Y and depleted in Ba, Sr and V (Vozárová in Marsina et al. 1999).

In petrological and geochemical composition, the Bučina Formation volcanites and volcaniclastics as well as zircon typology show a distinct similarity with the South-Gemeric rhyolite-dacite volcanism. Both represent a rift-related A-type magmatism (Šmelko 2007) connected with the Variscan post-orogenic extension and thermal relaxation. This coincides with the former results of Broska et al. (1993) based on zircon typology.

Monazite

Monazite, a REE bearing phosphate, is largely distributed in the studied rocks. Its grain size in the samples 1/SM, 2/SM (2nd volcanogenic horizon of the Rožňava Formation) and 3/SM (tectonic scale of the Bôrka Nappe) varies from 1 to 20 μm, while the crystals about 5–10 μm prevail. The monazites are mostly surrounded by the metamorphic white mica–phengite. In some places the columnar monazite is parallel oriented with the lepidoblastic orientation of the metamorphic mica (Fig. 4a). Most grains are angular, hypidiomorphic in shape (Fig. 4b,c). It seems that almost every small monazite grain is homogeneous in composition, although small size prevents a detailed observation of the zonality in BSE. Some zonality is observed only in a few larger grains (Fig. 4b,c). Dark zones located in the otherwise homogeneous monazite grains show unclear relations to the monazite shape or core-rim position. In Fig. 4b the dark zone can probably be interpreted as some type of oscillation growth (?). In Fig. 4c the dark zone occupies the center of the small monazite grain while the larger grain in the vicinity is fairly homogeneous. The dark zones are mostly free of Th or can reach only negligible concentrations below 0.5 wt. % resulting in large standard deviation of calculated chemical age.

The BEI images cannot reveal the zonality in single small monazites. The chemical composition between grains has quite substantial variability. Most of the chemical changes are attributed to the thorium. ThO_2 varies from very low concentrations of 0.9 wt. % up to 14.5 wt. % (5.1 wt. % in average). The uranium content is quite low; the UO_2 concentrations are between 0.023 and 0.735 wt. % (0.278 wt. % in average).

The monazites from the sample 4/SM (1st volcanogenic horizon of the Rožňava Formation) are different. The main feature is their concentric zonality (Fig. 4d,e,f). The resorbed lighter cores are surrounded by distinct dark zones which gradually transform into lighter broad rims. The monazites here are bigger than in previous samples (1, 2, 3/SM) having an average size of about 30–40 μm. Average concentration in ThO_2 is lower, ~3.5 wt. % and reaches up to 7.2 wt. %. The range in UO_2 concentration is comparable with other samples.

The chemical composition of the monazite from all samples recalculated to end-members is illustrated in Fig. 5. The major solid solution part of the crystal structure is filled by monazite-(Ce). The cheralite and huttonite content is even less. The monazite-(Ce) content is relatively high, 94.2 mol % in average (from 85.1 to 99.1 mol %). Almost pure monazite-(Ce) end-members are also present. The average huttonite content is low (1.5 mol %). Few monazites can contain up to 7.5 mol %. Cheralite content is higher than the huttonite, reaching 4.3 mol % on average with the range from 0 to 13.2 mol %.

The yttrium concentration in the majority of studied monazites is relatively low (between 0.3–0.5 wt. % Y_2O_3) suggesting subordinate xenotime-type substitutions. Elevated Y_2O_3 concentrations above 1.0 wt. % (up to 3.3 wt. %) have been encountered in a few monazites from sample 4/SM.

Dating results

The monazite chemical analyses and apparent ages from the Permian volcanic rocks of the Gočaltovo Group and Bučina Formation are listed in Table 1 and Table 2. All 48 apparent obtained ages are presented in the age histogram (Fig. 6). They are clearly separated into three main age populations: Silurian, Permian and Alpine. The oldest Silurian age records were found only in two monazite cores coming from the 1st volcanogenic horizon of the Rožňava Formation (sample 4/SM). Permian monazites are frequently present in the sample 4/SM and only one record has been found in the 2nd volcanogenic horizon of the Rožňava Formation (sample 2/SM). Alpine monazites are present in all the studied samples.

Sample ***1/SM***: the age is based on 8 points measured in 6 monazite grains giving a weighted average of 149 ± 30 Ma. The MSWD = 0.6 suggests a more concentrated data set relative to the normalized Gaussian distribution. Sample

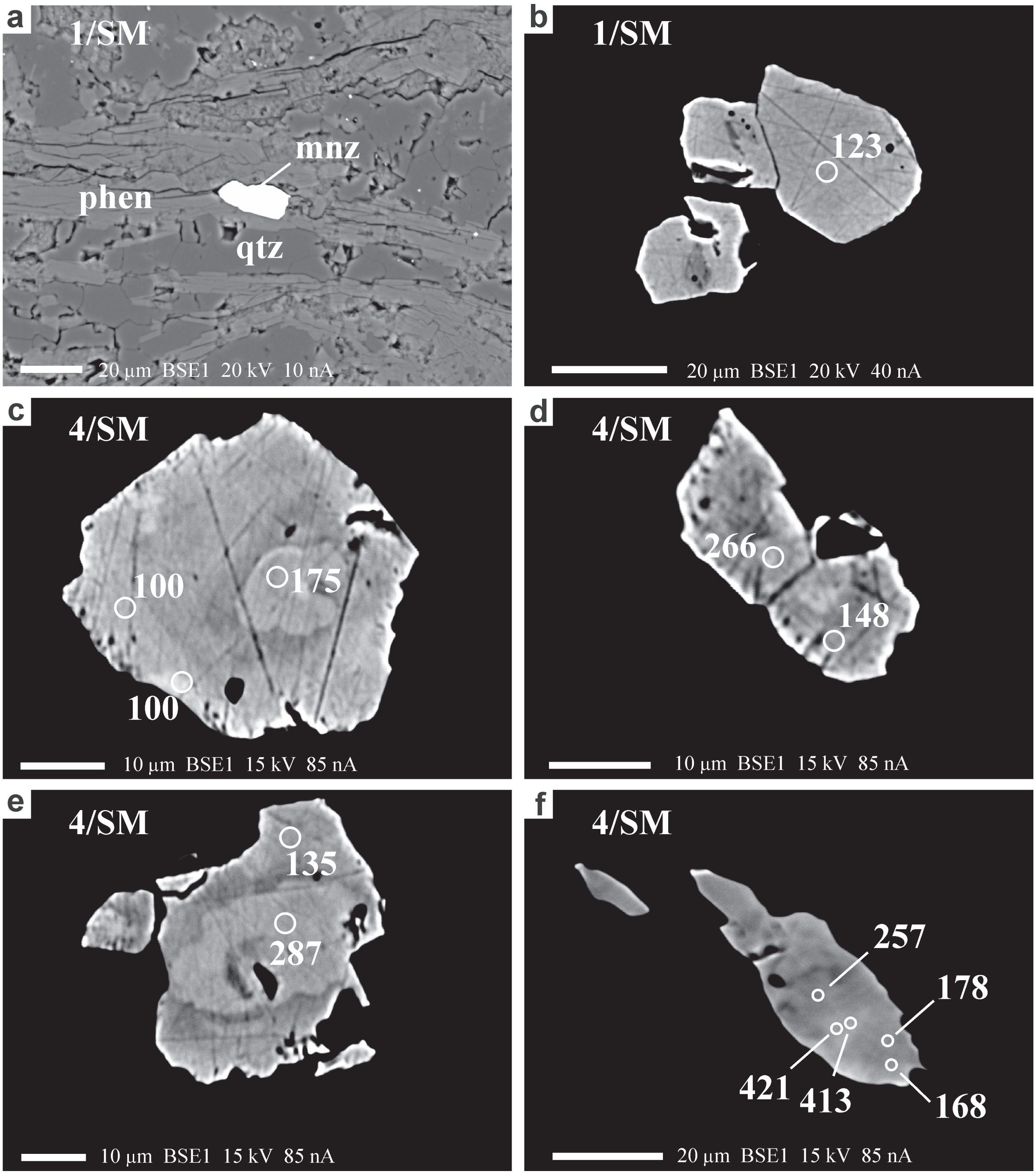

Fig. 4. BSE image of selected monazite grains. **a** — Irregular monazite grain surrounded by the metamorphic white mica-phengite (sample 1/SM); **b, c** — Dark zones in monazites having unclear relation to the mineral shape (sample 1/SM); **d** — Hypidiomorphic monazite grain with the lighter Jurassic core and the youngest Early Cretaceous rim (sample 4/SM); **e** — Hypidiomorphic monazite grain with the light Permian core and darker rim of Jurassic age (sample 4/SM); **f** — Irregular monazite grain with Permian core displaying of strong resorbtion and bordered by an Early Cretaceous rim (sample 4/SM).

2/SM: the weighted average of 15 points measured in 13 monazites gives 149 ± 10 Ma (MSWD = 0.39). Only one grain was less confidently dated to (?) Permian (264 ± 128 Ma), due to a large error resulting from a low Th content. Sample ***3/SM***: the chemical age obtained from 10 points measured in 9 monazite grains is 164 ± 26 Ma (MSWD = 0.43). Sample ***4/SM***: nine monazite grains were analysed; we obtained 22 point data which split into three age groups. The oldest Silurian group (2 grains) gives ages of 421 ± 95 and 413 ± 72 Ma. Silurian ages are always situated in the monazite cores. Permian data group (average = 275 ± 13 Ma, 8 grains) is always preserved in the light distinctly resorbed monazite cores. Young Alpine group ages has approximately the same range as in the other samples, giving the average age 147±25 Ma (9 grains). The two youngest ages ~100 Ma were revealed in the thin light

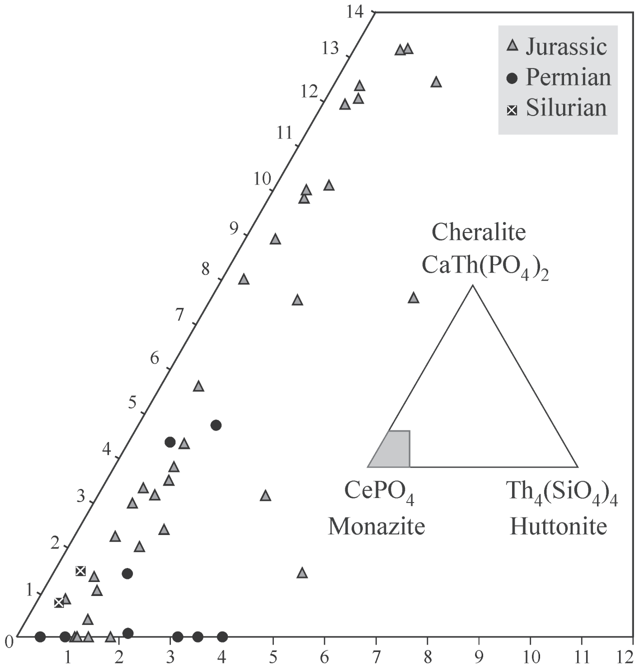

Fig. 5. Chemical composition of the monazite-(Ce) recalculated to monazite, brabantite and cheralite end-members (mol %). Jurassic monazites show strong huttonite substitution trend while Permian monazites define two trends, one to the huttonite and the other to the brabantite substitution trend. Silurian monazites approach composition close to the monazite end-member.

rim (Fig. 4d). Almost all monazites have corroded Permian cores surrounded by dark zone low in Th preventing reliable dating and subsequently rimmed by Alpine monazite.

Discussion

The Alpine tectonic evolution of the Western Carpathian internides is traditionally interpreted as a result of Cretaceous crustal shortening of Variscan basement crustal fragments and their Upper Paleozoic basin fillings associated with décollement of Upper Paleozoic-Mesozoic sedimentary sequences (Andrusov 1936, 1968; Andrusov et al. 1973; Plašienka et al. 1997). This fact was well documented by the radiometric ages of newly formed white mica from the Gemeric Unit ($^{40}Ar/^{39}Ar$ cooling ages ranging from 106 to 82 Ma, Dallmeyer et al. 1996; Vozárová et al. 2005, from W part of the Northern Gemericum) as well as the Early Cretaceous $^{40}Ar/^{39}Ar$ cooling ages from amphibole and paragonite from the vicinity of the Súľová granite body (140 Ma, Vozárová et al. 2000). The U-Th-Pb monazite ages from the uranium vein mineralization of the North-Gemeric Permian formation (124±10 Ma, Rojkovič & Konečný 2005), as well as from the quartz-stibnite veins penetrating the Southern Gemeric Early Paleozoic basement (120±9 Ma, Hurai et al. 2006), confirms fully this first stage of the polyphase Cretaceous collisional evolution in the Gemeric Unit. This collision event is well documented by the formation of the Gemer Cleavage Fan structure overprinting the pre-Mesozoic metamorphic fabric of the Northern and Southern Gemeric basements together with their Upper Paleozoic-Triassic cover formations as well as the Jurassic fabric of the Bôrka Nappe to the south (Lexa et al. 2003).

The strongly deformed and imbricated Permian-Mesozoic sequence of the Bôrka Nappe represents the bottom part of the Meliata Ocean accretionary wedge. It is formed by a system of thrust sheets consisting of thinned continental margin fragments (Permian clastics and volcanites, Triassic limestones and dolomites), deep-water sediments (?Triassic to Jurassic limestones and turbidites) and blueschist facies metabasalts (Mello et al. 1998). The Permian metasediments of the Bôrka Nappe, which were defined as the Bučina and Jasov Formations (Mello et al. 1998), have more lithological features in common with the Permian cover sequence of the Southern Gemeric basement represented by the Rožňava Formation of the Gočaltovo Group. They conspicuously differ from the Rožňava Formation by the substantially higher intensity of deformation and metamorphic recrystallization. The $^{40}Ar/^{39}Ar$ ages derived from metamorphic phengite yielded Late Jurassic ages for the Bôrka Nappe metamorphism (160–150 Ma; Maluski et al. 1993; Dallmeyer et al. 1996; Faryad & Henjes-Kunst 1997). This pre-Cretaceous tectonothermal event was connected with subduction-related processes of the Meliata Ocean, as well as formation of accretionary wedge (Mock et al. 1998; Mello et al. 1998) and its northwestward obduction over the Southern Gemeric basement (Mello et al. 1998; Lexa at al. 2003).

The monazite Th-U-Pb age data yield three populations (Fig. 6). The Alpine monazites with the average age of 150 Ma (weighted average $=148\pm8$ Ma, $n=37$, $MSWD=0.7$) recording the peak of the early Alpine metamorphism (Fig. 7). Alpine generation of monazites is present in all studied samples in the highest quantity. The frequency histogram of the Alpine ages in Fig. 6 shows slight bipolar distribution and relative large dispersion in the range of ages which may indicate at least two Alpine events. To separate these events, the Alpine ages were subjected to the statistical age data modeling based on minimizing the residual sums in the two sub-sets as described by Montel et al. (1996). The modeling assumes that the data sorted according to the increasing age are separated into two sub-sets at some age boundary. Mathematical test is a part of the used DAMON software (Patrik Konečný) used for the age calculations and handling. The Alpine ages were separated by statistical modeling at the 150 Ma border. The first subgroup of data with a weighted average age of 167 ± 12 Ma ($MSWD=0.17$, $n=17$, probability 1.0; Fig. 8) reflects the pre-Cretaceous tectonothermal event caused by the subduction of the Meliata Ocean. These obtained average ages show a good coincidence with the previous $^{40}Ar/^{39}Ar$ dating of metamorphic phengite from the Bôrka Nappe complex (160–150 Ma; Maluski et al. 1993; Dallmeyer et al. 1996; Faryad & Henjes-Kunst 1997). The second sub-group of the

Table 1: Representative analyses of the studied monazites from the samples 1/SM and 2/SM with calculated ages and chemical composition recalculated to end-members. *Continued on next page.*

sample analysis monazite	2/SM ana1 mnz1.1	2/SM ana2 mnz1.2	2/SM ana3 mnz2.1	2/SM ana4 mnz2.2	2/SM ana5 mnz3.1	2/SM ana7 mnz5.1	2/SM ana8 mnz6.1	2/SM ana9 mnz7.1	2/SM ana10 mnz8.1	2/SM ana11 mnz9.1	2/SM ana12 mnz10.1	2/SM ana13 mnz11.1	2/SM ana14 mnz12.1
SiO_2	0.2357	0.9745	0.1064	0.1259	0.2232	0.4029	0.1459	0.1566	0.2553	0.2567	0.1577	0.1708	0.4846
Al_2O_3	0.0008	0.1951	0.0000	0.0000	0.0070	0.0000	0.0000	0.0000	0.0000	0.0000	0.0000	0.0000	0.2286
La_2O_3	14.7021	12.8815	13.0494	12.7769	12.2319	12.5424	13.7665	12.5209	13.1883	12.3914	13.7631	13.4062	12.4772
Ce_2O_3	31.5168	27.7540	27.6954	27.5744	26.8281	27.1352	28.6472	27.5684	27.9883	26.7292	28.4325	28.4532	26.5256
Pr_2O_3	3.5714	3.0995	3.1684	3.1007	3.0847	3.0311	3.3127	3.0361	3.1705	3.0693	3.1632	3.1346	3.0269
Nd_2O_3	13.2834	11.6296	11.4207	11.5400	11.3920	11.5622	11.8565	11.8671	11.7608	11.5548	11.5565	11.7804	11.1386
$Sm2O_3$	2.5747	2.0637	2.1506	2.1207	2.3543	2.2827	2.2980	2.0838	2.3024	2.3246	2.0728	2.1979	2.2852
Eu_2O_3	0.0297	0.0544	0.0000	0.0652	0.0842	0.1060	0.0000	0.0000	0.0452	0.0000	0.0854	0.0838	0.0429
Gd_2O_3	1.7126	1.7138	1.5625	1.7206	1.6456	1.8524	1.6968	1.6979	1.7329	1.8751	1.5144	1.6899	1.8342
Tb_2O_3	0.0984	0.0606	0.0612	0.1310	0.0810	0.1191	0.0436	0.1125	0.0762	0.0560	0.0762	0.0679	0.0893
Dy_2O_3	0.0644	0.2003	0.2170	0.2374	0.3283	0.3009	0.2125	0.0000	0.2129	0.2936	0.1943	0.1938	0.1483
Ho_2O_3	0.0576	0.0149	0.0989	0.1052	0.1637	0.1441	0.1033	0.1905	0.0592	0.0759	0.0635	0.1832	0.0736
Er_2O_3	0.0000	0.1399	0.0000	0.0000	0.0206	0.0523	0.0000	0.0000	0.0000	0.0000	0.0000	0.0000	0.0000
Tm_2O_3	0.0000	0.0000	0.0000	0.0211	0.0000	0.0000	0.0000	0.0000	0.0000	0.0000	0.0000	0.0000	0.0000
Yb_2O_3	0.0024	0.0000	0.0330	0.0496	0.0256	0.0000	0.0608	0.0690	0.0514	0.0785	0.0010	0.0594	0.0241
Lu_2O_3	0.0000	0.0000	0.0000	0.0000	0.0000	0.0000	0.0531	0.0000	0.0000	0.0000	0.0119	0.0000	0.0256
PbO	0.0273	0.0616	0.0767	0.0653	0.0775	0.0720	0.0598	0.0688	0.0731	0.0737	0.0732	0.0679	0.0818
ThO_2	0.9689	6.3178	7.2914	7.2221	8.1099	7.0045	5.5268	7.4771	6.2819	7.6700	6.3301	6.4116	8.5117
UO_2	0.0535	0.5875	0.5281	0.5903	0.4695	0.6403	0.4918	0.5643	0.5782	0.6506	0.5041	0.4789	0.7353
Y_2O_3	0.3199	0.4313	0.4911	0.5093	0.5224	0.4931	0.3832	0.5234	0.4853	0.4385	0.4151	0.3928	0.3756
P_2O_5	28.7927	27.7583	28.7565	28.8853	28.6333	26.3348	29.0310	28.7887	28.8650	28.8624	28.8005	28.7903	28.1326
CaO	0.2418	1.3851	1.6190	1.7171	1.7638	1.4907	1.2717	1.6542	1.4060	1.7659	1.4056	1.4192	1.6792
As_2O_3	0.1672	0.1266	0.1395	0.1173	0.1301	0.1226	0.1261	0.1222	0.1283	0.1039	0.1609	0.1037	0.1345
Total	98.4213	97.4501	98.4657	98.6753	98.1767	95.6893	99.0874	98.5015	98.6611	98.2702	98.7820	99.0856	98.0553
cations recalculated to the base of 16 oxygens													
Si	0.0376	0.1562	0.0170	0.0199	0.0357	0.0674	0.0231	0.0250	0.0405	0.0410	0.0250	0.0271	0.0777
Al	0.0001	0.0368	0.0000	0.0000	0.0013	0.0000	0.0000	0.0000	0.0000	0.0000	0.0000	0.0000	0.0432
La	0.8638	0.7613	0.7696	0.7461	0.7223	0.7739	0.8050	0.7361	0.7725	0.7298	0.8052	0.7842	0.7383
Ce	1.8380	1.6283	1.6212	1.5983	1.5726	1.6619	1.6628	1.6089	1.6274	1.5626	1.6512	1.6520	1.5579
Pr	0.2073	0.1810	0.1846	0.1789	0.1800	0.1848	0.1914	0.1763	0.1835	0.1786	0.1828	0.1811	0.1769
Nd	0.7557	0.6656	0.6522	0.6525	0.6514	0.6908	0.6713	0.6756	0.6671	0.6590	0.6547	0.6672	0.6382
Sm	0.1411	0.1138	0.1183	0.1155	0.1297	0.1314	0.1254	0.1143	0.1258	0.1277	0.1131	0.1199	0.1261
Eu	0.0061	0.0113	0.0000	0.0134	0.0175	0.0230	0.0000	0.0000	0.0093	0.0000	0.0175	0.0172	0.0089
Gd	0.0904	0.0910	0.0828	0.0903	0.0873	0.1027	0.0892	0.0897	0.0912	0.0993	0.0796	0.0888	0.0975
Tb	0.0051	0.0032	0.0032	0.0068	0.0043	0.0065	0.0023	0.0059	0.0040	0.0029	0.0040	0.0035	0.0047
Dy	0.0033	0.0103	0.0112	0.0121	0.0169	0.0162	0.0109	0.0139	0.0109	0.0151	0.0099	0.0099	0.0077
Ho	0.0029	0.0008	0.0050	0.0053	0.0083	0.0077	0.0052	0.0097	0.0030	0.0039	0.0032	0.0092	0.0038
Er	0.0000	0.0070	0.0000	0.0000	0.0010	0.0027	0.0000	0.0000	0.0000	0.0000	0.0000	0.0000	0.0000
Tm	0.0000	0.0000	0.0000	0.0000	0.0000	0.0000	0.0000	0.0000	0.0000	0.0000	0.0000	0.0000	0.0000
Yb	0.0001	0.0000	0.0016	0.0024	0.0013	0.0000	0.0029	0.0034	0.0025	0.0038	0.0000	0.0029	0.0012
Lu	0.0000	0.0000	0.0000	0.0000	0.0000	0.0000	0.0025	0.0000	0.0000	0.0000	0.0006	0.0000	0.0012
Pb	0.0012	0.0027	0.0033	0.0028	0.0033	0.0032	0.0026	0.0030	0.0031	0.0032	0.0031	0.0029	0.0035
Th	0.0351	0.2304	0.2653	0.2602	0.2955	0.2667	0.1994	0.2712	0.2270	0.2787	0.2285	0.2314	0.3107
U	0.0020	0.0223	0.0200	0.0221	0.0178	0.0253	0.0184	0.0213	0.0217	0.0246	0.0189	0.0180	0.0279
Y	0.0271	0.0368	0.0418	0.0429	0.0445	0.0439	0.0323	0.0444	0.0410	0.0373	0.0350	0.0332	0.0321
P	3.8829	3.7657	3.8926	3.8715	3.8811	3.7297	3.8965	3.8850	3.8810	3.9018	3.8677	3.8654	3.8208
Ca	0.0413	0.2378	0.2774	0.2913	0.3026	0.2672	0.2160	0.2825	0.2393	0.3021	0.2389	0.2412	0.2886
As	0.0302	0.0230	0.0253	0.0211	0.0236	0.0233	0.0227	0.0221	0.0231	0.0188	0.0290	0.0187	0.0245
Total	7.9715	7.9852	7.9924	7.9532	7.9981	8.0283	7.9800	7.9883	7.9741	7.9901	7.9681	7.9738	7.9915
Σ REE	3.9140	3.4736	3.4497	3.4215	3.3926	3.6016	3.5688	3.4338	3.4972	3.3827	3.5220	3.5361	3.3624
huttonite	0.9	3.9	0.4	0.5	0.9	1.7	0.6	0.6	1.0	1.0	0.6	0.7	2.0
monazite	99.2	88.0	87.6	87.2	86.0	90.8	90.5	87.3	88.9	85.8	89.4	89.5	85.1
cheralite	0.0	7.6	11.9	12.3	13.1	7.5	8.9	12.0	10.1	13.2	10.0	9.8	12.4
age (Ma)	264±128	135±17.6	162±16.4	131±16.0	154±15.3	149±16.1	149±20.4	137±15.7	169±18.1	142±15.4	173±18.5	158±18.5	145±13.8

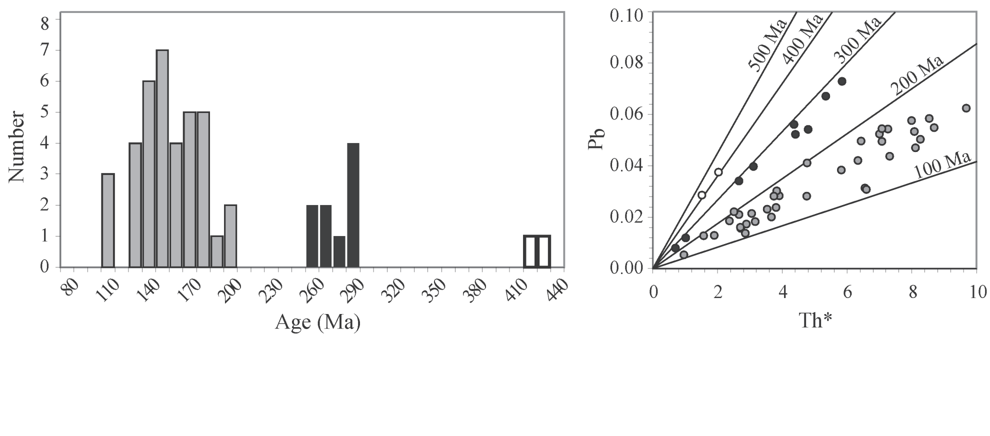

Fig. 6. The histogram and Pb vs. Th* illustrating three major events of monazite growth. Th* represents equivalent of Th increased by amount of U normalized to Th decay.

Table 1: *Continued.*

sample analysis monazite	1/SM ana3 mnz3.1	1/SM ana4 mnz4.1	1/SM ana5 mnz5.1	1/SM ana6 mnz6.1	1/SM ana7 mnz6.2	1/SM ana8 mnz7.1	1/SM ana9 mnz8.1
SiO_2	0.2740	0.2710	0.2881	0.2006	0.3440	0.1565	0.4123
Al_2O_3	0.0000	0.0246	0.0053	0.0000	0.0002	0.0000	0.0000
La_2O_3	15.0569	15.2080	14.5757	15.8862	14.7630	12.4078	14.3336
Ce_2O_3	31.1025	30.1861	30.7194	31.3195	30.8774	28.7966	30.1684
Pr_2O_3	3.3816	3.3242	3.2871	3.4112	3.4454	3.2200	3.4023
Nd_2O_3	12.2933	11.5618	12.0817	12.0598	12.4472	12.4163	12.5719
Sm2O3	1.9584	1.9756	2.1515	2.1286	2.3200	2.3113	2.2351
Eu_2O_3	0.0000	0.0000	0.0382	0.0076	0.0276	0.0000	0.0000
Gd_2O_3	1.3546	1.3744	1.4274	1.4573	1.5393	1.6385	1.5568
Tb_2O_3	0.0000	0.0604	0.0522	0.0767	0.0761	0.1347	0.0566
Dy_2O_3	0.0919	0.1530	0.2161	0.1598	0.2075	0.3472	0.2722
Ho_2O_3	0.1476	0.0616	0.2036	0.0648	0.0459	0.0821	0.3040
Er_2O_3	0.0000	0.0000	0.0835	0.0940	0.0000	0.0544	0.0232
Tm_2O_3	0.0000	0.0282	0.0000	0.0171	–0.0001	0.0000	0.0000
Yb_2O_3	0.0902	0.1039	0.0090	0.0595	0.0184	0.0087	0.0278
Lu_2O_3	0.0000	0.0000	0.0000	0.0000	0.0000	0.0000	0.0000
PbO	0.0362	0.0471	0.0450	0.0320	0.0343	0.0478	0.0394
ThO_2	3.9671	4.0518	3.8847	2.9513	3.4238	6.3280	3.8520
UO_2	0.0583	0.0907	0.1085	0.0376	0.0521	0.3457	0.0489
Y_2O_3	0.2974	0.3149	0.3873	0.3139	0.3782	0.4785	0.3924
P_2O_5	28.5143	28.3775	28.6523	28.7769	28.4491	28.4701	28.1663
CaO	0.6980	0.8033	0.6983	0.6386	0.5013	1.3493	0.5927
As_2O_3	0.1599	0.1804	0.1270	0.1518	0.1419	0.1512	0.1767
Total	99.4822	98.1985	99.0419	99.8448	99.0925	98.7446	98.6326
cations recalculated to the base of 16 oxygens							
Si	0.0435	0.0433	0.0457	0.0315	0.0546	0.0250	0.0661
Al	0.0000	0.0046	0.0010	0.0000	0.0000	0.0000	0.0000
La	0.8815	0.8965	0.8533	0.9222	0.8649	0.7313	0.8471
Ce	1.8074	1.7663	1.7852	1.8046	1.7957	1.6848	1.7698
Pr	0.1956	0.1936	0.1901	0.1956	0.1994	0.1875	0.1986
Nd	0.6969	0.6599	0.6849	0.6779	0.7062	0.7086	0.7194
Sm	0.1070	0.1086	0.1175	0.1153	0.1268	0.1271	0.1232
Eu	0.0000	0.0000	0.0078	0.0015	0.0057	0.0000	0.0000
Gd	0.0713	0.0728	0.0751	0.0760	0.0811	0.0868	0.0827
Tb	0.0000	0.0032	0.0027	0.0040	0.0040	0.0071	0.0030
Dy	0.0047	0.0079	0.0111	0.0081	0.0106	0.0179	0.0141
Ho	0.0074	0.0031	0.0103	0.0032	0.0023	0.0042	0.0155
Er	0.0000	0.0000	0.0042	0.0046	0.0000	0.0027	0.0012
Tm	0.0000	0.0059	0.0000	0.0035	0.0000	0.0000	0.0000
Yb	0.0044	0.0051	0.0004	0.0029	0.0009	0.0004	0.0014
Lu	0.0000	0.0000	0.0000	0.0000	0.0000	0.0000	0.0000
Pb	0.0015	0.0020	0.0019	0.0014	0.0015	0.0021	0.0017
Th	0.1433	0.1474	0.1403	0.1057	0.1238	0.2301	0.1405
U	0.0022	0.0034	0.0041	0.0014	0.0020	0.0131	0.0019
Y	0.0251	0.0268	0.0327	0.0263	0.0320	0.0407	0.0335
P	3.8317	3.8395	3.8503	3.8342	3.8259	3.8518	3.8208
Ca	0.1187	0.1376	0.1187	0.1077	0.0853	0.2311	0.1018
As	0.0288	0.0327	0.0229	0.0271	0.0256	0.0274	0.0321
Total	7.9711	7.9602	7.9603	7.9548	7.9482	7.9796	7.9741
Σ REE	3.7762	3.7228	3.7427	3.8194	3.7976	3.5584	3.7759
huttonite	1.1	1.1	1.2	0.8	1.4	0.6	1.7
monazite	95.7	94.5	95.0	97.0	96.6	90.5	95.9
cheralite	3.2	4.3	3.8	2.2	2.0	8.9	2.4
age (Ma)	123±34.2	177±33.4	170±34.3	134±46.6	130±39.9	–	148±35.8

age data set had a weighted average age of 136±10 Ma (MSWD=0.37, n=20, probability=0.99; Fig. 9). This average value reflects starting of the Early Cretaceous polyphase structural evolution, which was evoked by the successive collision and indentation in the Inner Western Carpathians.

The youngest ~100 Ma light coloured rims surrounding the monazite grains from the 1st volcanogenic horizon of the Rožňava Formation (sample 4/SM, Fig. 4d) are genetically related to the proceeded Cretaceous compression stage, associated within the Southern Gemeric Unit with the development of the Gemer Cleavage Fan (according to Lexa et al. 2003).

The chemical age data of the monazite from Gočaltovo Formation metavolcanites also confirm the record of the paleo-Alpine tectonothermal event in the Southern Gemeric Unit, which coincided with the formation of the Meliata Ocean accretionary wedge. In fact, the Permian metasediments and metavolcanites of the Southern Gemeric Unit show distinct crystallization schistosity and flattening of coarse clasts, which are parallel to the well preserved sedimentary bedding. Thus, the high-pressure metamorphosed tectonic scales of the Bučina and Jasov Formations of the Bôrka Nappe represent thrust sheets of the thinned continental margin which is consistent with the Southern Gemeric cover. These are lithologically and mineralogically consistent with the Permian coarse-grained envelope sequence of the Southern Gemeric Unit (Reichwalder 1973; Bajaník et al. 1981, 1983, 1984). Evidence of the Late Jurassic monazite ages (150–160 Ma) from the metavolcanites of the Gočaltovo Group allow us to state that the thinned continental margin represented by the Southern Gemeric basement and its Permian envelope was intensively reworked during Late Jurassic as a response of subduction/accretion processes and closing of the Meliata Ocean. These results fully confirmed the suggestions derived from structural analysis presented by Lexa et al. (2003).

Since the stage of deformation and metamorphic recrystallization of the Rožňava Formation sedimentary complexes did not reach high-pressure conditions, it is difficult to presuppose that it was dragged into the Meliata subduction zone. The Late

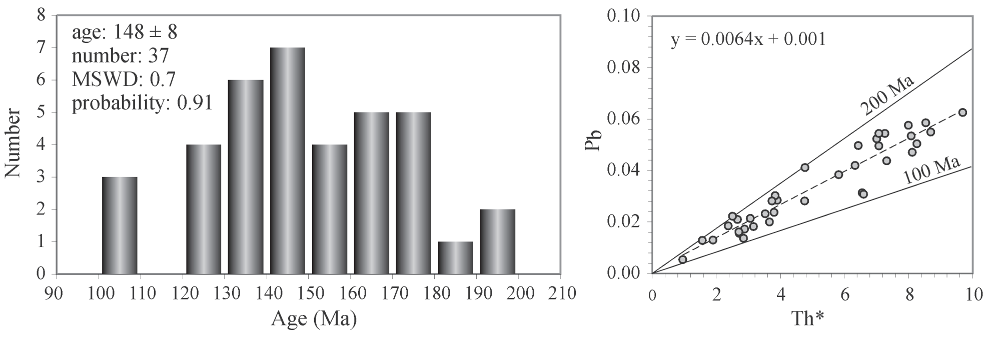

Fig. 7. Histogram and isochrone of the monazite ages for the whole Alpine populations.

Table 2: Representative analyses of studied monazites from the samples 3/SM and 4/SM with calculated ages and chemical composition recalculated to end-members. *Continued on next page.*

sample	3-SM	3-SM	3-SM	3-SM	3-SM	3-SM	3-SM	3-SM	4-SM	4-SM	4-SM	4-SM	4-SM	4-SM
analysis	**ana1**	**ana2**	**ana3**	**ana4**	**ana6**	**ana8**	**ana9**	**ana10**	**ana1**	**ana2**	**ana3**	**ana4**	**ana5**	**ana6**
monazite	**mnz1.1**	**mnz2.1**	**mnz3.1**	**mnz4.1**	**mnz6.1**	**mnz8.1**	**mnz9.1**	**mnz10.1**	**mnz1.1**	**mnz1.2**	**mnz1.3**	**mnz1.4**	**mnz1.5**	**mnz2.1**
SiO_2	0.3475	0.2981	0.1863	0.2864	1.1883	0.2973	0.2914	1.7352	0.1089	0.1052	0.1325	0.1168	0.1257	0.2095
Al_2O_3	0.0159	0.0068	0.0000	0.0002	0.0125	0.0129	0.0150	0.0305	0.0000	0.0000	0.0000	0.0000	0.0000	0.0000
La_2O_3	13.5139	13.8753	14.7592	15.2893	11.6202	12.9650	14.2799	9.2868	18.4262	13.2191	15.0646	18.0868	16.6193	13.4042
Ce_2O_3	29.7213	29.6748	30.7499	32.2334	28.1722	29.7341	30.2576	23.0077	31.5717	28.4002	31.1357	32.6622	31.4545	29.5411
Pr_2O_3	3.9988	3.8747	3.5453	3.6558	3.6539	3.7204	3.8236	3.3452	3.3328	3.6348	3.6355	3.6623	3.6480	3.8124
Nd_2O_3	15.2010	15.6148	12.0879	12.9243	14.8634	13.0363	13.9884	15.3108	11.0971	12.4331	12.7786	11.6251	12.1172	13.9368
Sm_2O_3	2.4836	2.9042	1.7677	2.1892	2.5346	2.2299	2.2400	3.7952	1.6588	2.3388	2.2423	1.8834	1.9675	2.6978
Eu_2O_3	0.2534	0.1519	0.0241	0.2217	0.1474	0.0649	0.2076	0.1807	0.0171	0.0855	0.0545	0.0279	0.0192	0.0000
Gd_2O_3	2.0108	2.1392	1.5753	1.7169	1.7074	1.6245	1.7529	2.1099	1.4718	2.2416	2.0955	1.6093	1.6626	2.4945
Tb_2O_3	0.0000	0.0094	0.1000	0.0022	0.0502	0.0022	0.0000	0.0516	0.0517	0.1264	0.1054	0.0000	0.0575	0.0813
Dy_2O_3	0.1876	0.2732	0.0448	0.3241	0.2171	0.2574	0.3069	0.2317	0.1304	0.1789	0.3302	0.0000	0.1130	0.2653
Ho_2O_3	0.2187	0.1950	0.1230	0.1903	0.1352	0.1272	0.1687	0.0447	0.2426	0.1372	0.1198	0.1899	0.0694	0.2047
Er_2O_3	0.0000	0.0923	0.0162	0.0207	0.0000	0.0223	0.1913	0.0000	0.1709	0.0000	0.0552	0.0193	0.0000	0.0000
Tm_2O_3	0.0000	0.0000	0.0341	0.0000	0.0000	0.0000	0.0000	0.0000	0.0000	0.0413	0.0810	0.0000	0.0000	0.0292
Yb_2O_3	0.0721	0.1035	0.0438	0.0000	0.0000	0.1115	0.0000	0.0873	0.0859	0.0000	0.0889	0.1163	0.0696	0.0000
Lu_2O_3	0.0000	0.0000	0.0000	0.0000	0.0000	0.0000	0.0458	0.2725	0.0941	0.0000	0.0000	0.0000	0.0000	0.2688
PbO	0.0262	0.0259	0.0427	0.0180	0.0656	0.0425	0.0290	0.1414	0.0431	0.0686	0.0348	0.0208	0.0525	0.0353
ThO_2	2.0416	1.7106	3.8571	1.0173	7.0349	4.8901	2.8736	14.5802	1.6593	5.1000	1.4365	0.7544	2.2074	3.0830
UO_2	0.0358	0.0230	0.1829	0.0227	0.0891	0.1630	0.0695	0.3525	0.0211	0.8917	0.4946	0.0565	0.0600	0.1234
Y_2O_3	0.2739	0.2813	0.3900	0.4287	0.3934	0.5686	0.3570	0.6271	0.1793	0.4986	0.5072	0.1523	0.2057	0.6117
P_2O_5	27.8361	27.7677	27.8185	27.9973	26.5169	27.2912	27.9435	24.4294	28.9154	28.6343	28.8528	28.5133	28.9038	28.3655
CaO	0.3157	0.3232	0.8745	0.4815	0.7677	1.1321	0.4440	1.2133	0.5198	1.4006	0.4591	0.1617	0.5776	0.5560
FeO	0.0282	0.0788	0.0000	0.0000	0.0636	0.0774	0.1345	0.0350	0.0202	0.0000	0.0000	0.0127	0.0000	0.0000
SO_2	0.0345	0.0771	0.1047	0.2057	0.1620	0.1904	0.0884	0.0709	0.1925	0.1584	0.0648	0.0351	0.1126	0.0400
TiO_2	0.0000	0.0000	0.6340	0.0000	0.0000	0.0000	0.0000	0.6706	0.0000	0.0000	0.0000	0.0000	0.0000	0.0000
As_2O_5	0.2074	0.2483	0.1881	0.2220	0.2005	0.1577	0.2142	0.1744	0.1454	0.1370	0.1512	0.1460	0.1783	0.3466
Total	98.8240	99.7492	99.1500	99.4478	99.5962	98.7189	99.7229	101.7844	100.1562	99.8314	99.9208	99.8521	100.2215	100.1072
cations recalculated to the base of 16 oxygens														
Si	0.0568	0.0486	0.0302	0.0463	0.1953	0.0489	0.0473	0.2898	0.0173	0.0169	0.0212	0.0188	0.0200	0.0338
Al	0.0031	0.0013	0.0000	0.0000	0.0024	0.0025	0.0029	0.0060	0.0000	0.0000	0.0000	0.0000	0.0000	0.0000
La	0.8154	0.8340	0.8817	0.9126	0.7043	0.7859	0.8549	0.5720	1.0826	0.7827	0.8898	1.0748	0.9777	0.7966
Ce	1.7800	1.7706	1.8234	1.9098	1.6949	1.7891	1.7980	1.4067	1.8413	1.6691	1.8256	1.9267	1.8367	1.7427
Pr	0.2383	0.2301	0.2092	0.2156	0.2188	0.2228	0.2261	0.2036	0.1934	0.2126	0.2121	0.2150	0.2120	0.2238
Nd	0.8881	0.9089	0.6992	0.7470	0.8723	0.7652	0.8109	0.9132	0.6313	0.7128	0.7309	0.6689	0.6902	0.8020
Sm	0.1401	0.1632	0.0987	0.1221	0.1436	0.1263	0.1253	0.2185	0.0911	0.1294	0.1238	0.1046	0.1082	0.1499
Eu	0.0142	0.0085	0.0013	0.0122	0.0083	0.0036	0.0115	0.0103	0.0009	0.0047	0.0030	0.0015	0.0010	0.0000
Gd	0.1090	0.1156	0.0846	0.0921	0.0930	0.0885	0.0943	0.1168	0.0777	0.1193	0.1112	0.0860	0.0879	0.1332
Tb	0.0000	0.0005	0.0053	0.0001	0.0027	0.0001	0.0000	0.0028	0.0027	0.0067	0.0055	0.0000	0.0030	0.0043
Dy	0.0099	0.0143	0.0023	0.0169	0.0115	0.0136	0.0160	0.0125	0.0067	0.0093	0.0170	0.0000	0.0058	0.0138
Ho	0.0114	0.0101	0.0063	0.0098	0.0071	0.0067	0.0087	0.0024	0.0123	0.0070	0.0061	0.0097	0.0035	0.0105
Er	0.0000	0.0047	0.0008	0.0011	0.0000	0.0012	0.0098	0.0000	0.0086	0.0000	0.0028	0.0010	0.0000	0.0000
Tm	0.0000	0.0000	0.0017	0.0000	0.0000	0.0000	0.0000	0.0000	0.0000	0.0021	0.0040	0.0000	0.0000	0.0015
Yb	0.0036	0.0051	0.0022	0.0000	0.0000	0.0056	0.0000	0.0044	0.0042	0.0000	0.0043	0.0057	0.0034	0.0000
Lu	0.0000	0.0000	0.0000	0.0000	0.0000	0.0000	0.0022	0.0137	0.0045	0.0000	0.0000	0.0000	0.0000	0.0131
Pb	0.0012	0.0011	0.0019	0.0008	0.0029	0.0019	0.0013	0.0064	0.0018	0.0030	0.0015	0.0009	0.0023	0.0015
Th	0.0760	0.0634	0.1422	0.0375	0.2631	0.1829	0.1061	0.5541	0.0602	0.1863	0.0524	0.0277	0.0801	0.1130
U	0.0013	0.0008	0.0066	0.0008	0.0033	0.0060	0.0025	0.0131	0.0007	0.0319	0.0176	0.0020	0.0021	0.0044
Y	0.0238	0.0244	0.0336	0.0369	0.0344	0.0497	0.0308	0.0557	0.0152	0.0426	0.0432	0.0131	0.0175	0.0525
P	3.8551	3.8312	3.8145	3.8358	3.6890	3.7973	3.8398	3.4539	3.8996	3.8915	3.9119	3.8893	3.9029	3.8694
Ca	0.0553	0.0564	0.1518	0.0835	0.1352	0.1994	0.0772	0.2171	0.0887	0.2409	0.0788	0.0279	0.0987	0.0960
Fe^{2+}	0.0039	0.0107	0.0000	0.0000	0.0087	0.0106	0.0183	0.0049	0.0027	0.0000	0.0000	0.0017	0.0000	0.0000
S	0.0053	0.0118	0.0159	0.0312	0.0250	0.0293	0.0135	0.0111	0.0288	0.0238	0.0097	0.0053	0.0168	0.0060
Ti	0.0000	0.0000	0.0772	0.0000	0.0000	0.0000	0.0000	0.0842	0.0000	0.0000	0.0000	0.0000	0.0000	0.0000
As	0.0177	0.0212	0.0159	0.0188	0.0172	0.0136	0.0182	0.0152	0.0121	0.0115	0.0127	0.0123	0.0149	0.0292
Suma kat	8.1095	8.1365	8.1066	8.1309	8.1329	8.1507	8.1157	8.1885	8.0846	8.1040	8.0853	8.0929	8.0848	8.0973
Σ REE	4.0100	4.0656	3.8169	4.0393	3.7564	3.8087	3.9556	3.4632	3.9529	3.6556	3.9363	4.0939	3.9295	3.8783
huttonite	1.4	1.2	0.8	1.1	4.8	1.2	1.2	7.2	0.4	0.4	0.5	0.5	0.5	0.8
monazite	98.6	98.8	96.3	98.9	93.7	95.3	98.8	87.4	98.8	91.6	98.6	99.5	98.0	97.8
cheralite	0	0	3.0	0	1.4	3.5	0	5.4	0.8	8.0	0.9	0	1.5	1.3
age (Ma)	154±72.5	183±86.2	163±35.1	127±138	173±22.1	133±28.8	129±49.8	195±11	421±95.7	168±20.3	178±51.3	257±202.6	413±72	158±44.9

Jurassic sub-group of monazites, which were found in the Southern Gemeric Permian metavolcanites, reflects, most probably, the influence of subduction derived fluids. They could penetrate a relative wide zone of continental margin along the subduction/accretion belt. This interpretation allows us to change our opinion on the vergency of the Jurassic subduction-related compressional event in the Western Carpathians. The presented monazite age data assign the Southern Gemeric Unit to the active continental margin of the Meliata Ocean. Further relevant evidence is being collected.

Minor monazite data derived from metavolcanites of the 1st volcanogenic horizon of the southgemeric envelope complex of the Rožňava Formation (sample 4/SM)

Table 2: *Continued.*

sample	4-SM	4-SM	4-SM	4-SM	4-SM	4-SM	4-SM	4-SM	4-SM	4-SM	4-SM	4-SM	4-SM
analysis	ana9	ana10	ana11	ana12	ana13	ana14	ana15	ana16	ana17	ana18	ana21	ana21	ana22
monazite	mnz3.2	mnz4.1	mnz4.2	mnz4.3	mnz5.1	mnz5.2	mnz6.1	mnz7.1	mnz7.2	mnz8.1	mnz8.4	mnz8.4	mnz9.1
SiO_2	0.1996	0.9146	1.0041	0.1819	0.2051	0.3785	0.3612	0.8145	0.2611	0.4676	0.2950	0.8036	0.5296
Al_2O_3	0.0000	0.0000	0.0000	0.0000	0.0000	0.0000	0.0000	0.0000	0.0000	0.0000	0.0000	0.0000	0.0000
La_2O_3	15.3035	10.5174	9.2010	13.8682	14.1889	14.0013	11.9096	17.3898	15.5230	15.2638	14.8177	12.0145	14.8823
Ce_2O_3	29.7262	26.9307	25.7944	29.2500	28.7295	28.9098	27.1836	31.4579	30.0552	30.6924	29.6884	27.3892	29.9298
Pr_2O_3	3.4436	3.7389	3.7563	3.3998	3.4499	3.5789	3.5730	3.6518	3.7320	3.7946	3.6735	3.6491	3.5412
Nd_2O_3	12.5525	14.8325	14.8233	12.6837	12.7941	12.8678	14.1379	12.3875	12.7543	13.6005	13.1167	13.5486	13.2976
Sm_2O_3	2.2587	3.3782	3.3313	2.0965	2.2697	2.2371	2.8389	1.4105	2.4866	1.8519	2.7575	3.2067	1.7952
Eu_2O_3	0.0000	0.0000	0.0000	0.0000	0.0000	0.1338	0.0000	0.0000	0.0000	0.0000	0.0499	0.0104	0.0000
Gd_2O_3	1.8910	3.1329	3.1267	2.1238	2.4152	2.0549	2.5996	1.3380	2.2433	1.6968	2.3538	2.7133	1.5157
Tb_2O_3	0.0708	0.2777	0.1992	0.1100	0.1789	0.0588	0.1974	0.0269	0.0394	0.0567	0.0275	0.0575	0.0237
Dy_2O_3	0.1470	1.0980	1.2678	0.1264	0.4339	0.2015	0.8046	0.3566	0.1767	0.4749	0.2273	0.3833	0.3291
Ho_2O_3	0.2551	0.2411	0.2616	0.1092	0.0264	0.0378	0.2241	0.2931	0.0652	0.1584	0.2882	0.1056	0.1485
Er_2O_3	0.0000	0.2413	0.2290	0.0000	0.0000	0.0112	0.0000	0.0000	0.0072	0.0367	0.0000	0.0000	0.0070
Tm_2O_3	0.0000	0.0332	0.0041	0.0284	0.0000	0.0277	0.0608	0.0000	0.0236	0.0000	0.0000	0.0000	0.0000
Yb_2O_3	0.0000	0.1540	0.1573	0.0876	0.0413	0.0800	0.0299	0.1444	0.0593	0.1175	0.0000	0.0623	0.0814
Lu_2O_3	0.0199	0.0162	0.0376	0.0000	0.2322	0.0000	0.0787	0.0000	0.0608	0.0000	0.0000	0.0234	0.0000
PbO	0.0378	0.0706	0.0684	0.0534	0.0844	0.0907	0.0726	0.0490	0.0308	0.0321	0.0269	0.0459	0.0549
ThO_2	3.8540	4.8085	4.2976	5.2100	4.8789	5.4011	4.5615	2.9000	3.1676	2.5672	3.1340	7.1753	3.3755
UO_2	0.1478	0.2016	0.2205	0.4415	0.3686	0.3846	0.1225	0.0395	0.0362	0.0724	0.0358	0.0896	0.0395
Y_2O_3	0.2683	3.3274	3.1914	0.4080	1.2304	0.4094	2.4007	0.5524	0.3192	1.1383	0.3445	0.4383	1.0188
P_2O_5	28.4444	27.4593	27.9354	27.9892	28.5660	27.9701	27.7474	27.8143	28.3014	28.1301	27.9961	27.0243	27.9728
CaO	0.7808	0.2913	0.3265	1.2736	1.0493	1.0914	0.6828	0.1477	0.5881	0.3229	0.4704	0.8270	0.4001
FeO	0.0000	0.0000	0.0000	0.0000	0.0000	0.0000	0.0000	0.0000	0.0252	0.0000	0.0000	0.0000	0.0000
SO_2	0.0670	0.0000	0.0048	0.0776	0.0191	0.0006	0.0013	0.0076	0.0606	0.0043	0.0188	0.0267	0.0133
TiO_2	0.0000	0.0000	0.0000	0.0000	0.0000	0.0000	0.0000	0.0000	0.0000	0.0000	0.0000	0.0000	0.0000
As_2O_5	0.1802	0.1887	0.1419	0.1591	0.1531	0.1311	0.1861	0.1489	0.2651	0.1809	0.2520	0.2582	0.1500
Total	99.6482	101.8543	99.3802	99.6779	101.3149	100.0582	99.7744	100.9303	100.2820	100.6599	99.5741	99.8528	99.1061
cations recalculated to the base of 16 oxygens													
Si	0.0322	0.1467	0.1618	0.0295	0.0327	0.0613	0.0587	0.1307	0.0420	0.0750	0.0480	0.1319	0.0859
Al	0.0000	0.0000	0.0000	0.0000	0.0000	0.0000	0.0000	0.0000	0.0000	0.0000	0.0000	0.0000	0.0000
La	0.9104	0.6221	0.5469	0.8299	0.8339	0.8364	0.7136	1.0290	0.9216	0.9032	0.8889	0.7276	0.8900
Ce	1.7553	1.5812	1.5218	1.7374	1.6761	1.7142	1.6169	1.8477	1.7712	1.8028	1.7678	1.6464	1.7766
Pr	0.2024	0.2185	0.2206	0.2010	0.2003	0.2112	0.2115	0.2135	0.2189	0.2218	0.2177	0.2183	0.2092
Nd	0.7231	0.8495	0.8531	0.7349	0.7281	0.7443	0.8203	0.7098	0.7332	0.7793	0.7619	0.7945	0.7700
Sm	0.1256	0.1868	0.1851	0.1173	0.1247	0.1249	0.1590	0.0780	0.1380	0.1024	0.1546	0.1815	0.1003
Eu	0.0000	0.0000	0.0000	0.0000	0.0000	0.0074	0.0000	0.0000	0.0000	0.0000	0.0028	0.0006	0.0000
Gd	0.1011	0.1666	0.1670	0.1142	0.1276	0.1103	0.1400	0.0712	0.1197	0.0902	0.1269	0.1477	0.0815
Tb	0.0038	0.0146	0.0105	0.0059	0.0094	0.0031	0.0105	0.0014	0.0021	0.0030	0.0015	0.0031	0.0013
Dy	0.0076	0.0567	0.0658	0.0066	0.0223	0.0105	0.0421	0.0184	0.0092	0.0245	0.0119	0.0203	0.0172
Ho	0.0131	0.0123	0.0134	0.0056	0.0013	0.0019	0.0116	0.0150	0.0033	0.0081	0.0149	0.0055	0.0077
Er	0.0000	0.0122	0.0116	0.0000	0.0000	0.0006	0.0000	0.0000	0.0004	0.0018	0.0000	0.0000	0.0004
Tm	0.0000	0.0017	0.0002	0.0014	0.0000	0.0014	0.0031	0.0000	0.0012	0.0000	0.0000	0.0000	0.0000
Yb	0.0000	0.0075	0.0077	0.0043	0.0020	0.0040	0.0015	0.0071	0.0029	0.0057	0.0000	0.0031	0.0040
Lu	0.0010	0.0008	0.0018	0.0000	0.0112	0.0000	0.0039	0.0000	0.0030	0.0000	0.0000	0.0012	0.0000
Pb	0.0016	0.0030	0.0030	0.0023	0.0036	0.0040	0.0032	0.0021	0.0013	0.0014	0.0012	0.0020	0.0024
Th	0.1415	0.1755	0.1576	0.1924	0.1769	0.1991	0.1686	0.1059	0.1160	0.0937	0.1160	0.2681	0.1245
U	0.0053	0.0072	0.0079	0.0159	0.0131	0.0139	0.0044	0.0014	0.0013	0.0026	0.0013	0.0033	0.0014
Y	0.0230	0.2840	0.2737	0.0352	0.1043	0.0353	0.2076	0.0472	0.0273	0.0972	0.0298	0.0383	0.0879
P	3.8840	3.7280	3.8111	3.8444	3.8537	3.8351	3.8165	3.7778	3.8567	3.8207	3.8549	3.7564	3.8397
Ca	0.1349	0.0501	0.0564	0.2214	0.1792	0.1894	0.1189	0.0254	0.1014	0.0555	0.0820	0.1455	0.0695
Fe^{2+}	0.0000	0.0000	0.0000	0.0000	0.0000	0.0000	0.0000	0.0000	0.0034	0.0000	0.0000	0.0000	0.0000
S	0.0101	0.0000	0.0007	0.0118	0.0029	0.0001	0.0002	0.0011	0.0091	0.0006	0.0029	0.0041	0.0020
Ti	0.0000	0.0000	0.0000	0.0000	0.0000	0.0000	0.0000	0.0000	0.0000	0.0000	0.0000	0.0000	0.0000
As	0.0152	0.0158	0.0120	0.0135	0.0128	0.0111	0.0158	0.0125	0.0223	0.0152	0.0214	0.0222	0.0127
Suma kat	8.0912	8.1406	8.0897	8.1249	8.1160	8.1193	8.1279	8.0950	8.1055	8.1049	8.1063	8.1214	8.0842
Σ REE	3.8423	3.7295	3.6037	3.7585	3.7257	3.7702	3.7302	3.9910	3.9216	3.9429	3.9489	3.7485	3.8581
huttonite	0.8	3.5	4.0	0.7	0.8	1.5	1.4	3.1	1.0	1.8	1.2	3.3	2.1
monazite	95.9	96.5	96.0	93.7	94.8	93.8	97.1	96.9	97.9	98.2	98.4	93.6	97.8
cheralite	3.3	0	0	5.6	4.4	4.7	1.4	0	1.0	0	0.4	3.2	0.1
age (Ma)	141±36.4	253±30.4	266±33.6	148±23.8	282±27.6	280±25.2	288±33.5	287±53.4	135±47.5	175±58.2	108±47.2	108±21.1	286±46.3

confirm the weighted average age 276 ± 25 Ma (MSWD = 0.12, n = 9; Fig. 10). The isochrone in Fig. 10 intercepting the zero confirms the reliability of the monazite chemical dating. The first detected age data represent the magmatic event passed during the Early Permian within the rifted South-Gemeric basement. This volcanic activity was related to the Variscan late-orogenic collapse and rifting in the foreland, which expanded within the external part of the Western Carpathian Variscides during Early Permian.

The preserved Silurian monazite age data from the 1st volcanogenic horizon of the Rožňava Formation (sample 4/SM) most probably derive from inherited cores trapped in the Permian magmatic monazite grains. Their direct

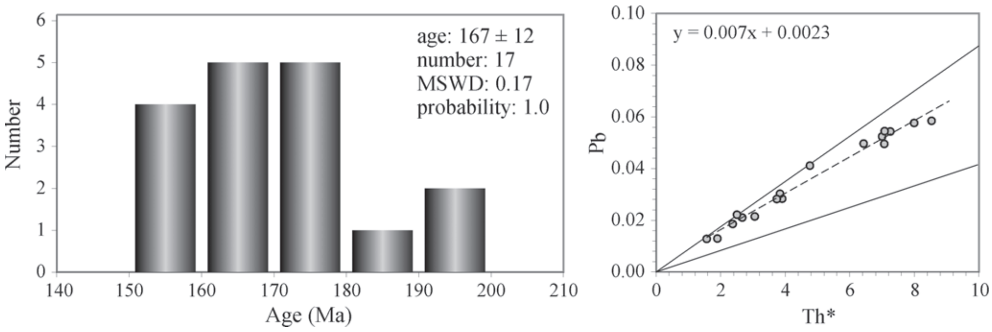

Fig. 8. Histogram and isochrone of the Jurassic population of monazites.

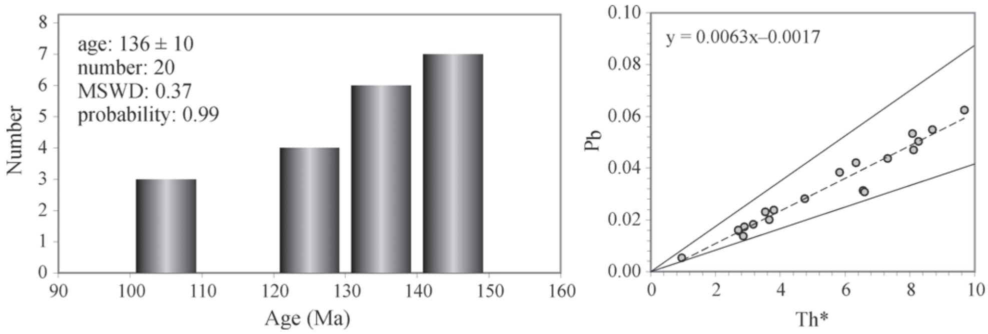

Fig. 9. Histogram and isochrone of the Early Cretaceous population of monazite.

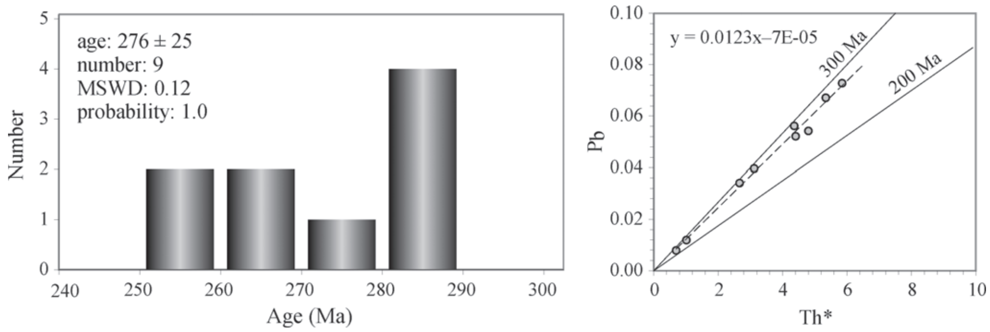

Fig. 10. Histogram and isochrone of the Permian population of monazite.

provenance from the underlying Lower Paleozoic protolith is highly probable.

Conclusions

The Early Permian magmatic event at 276±25 Ma has been determined for the first time from the Rožňava Formation volcanites. This volcanic activity was connected with the late Variscan rifting as a response to the foreland collapse of the Western Carpathian Variscan collision belt. Isolated relics of the Silurian ages (421 and 431 Ma) found within the Permian monazite cores are interpreted as the inherited relict from the source rocks, extracted probably from the Lower Paleozoic protolith.

Chemical monazite dating from the Permian metavolcanites and metavolcaniclastics of the Southern Gemeric Gočaltovo Group and Bôrka Nappe records the Late Jurassic tectonothermal overprinting. The sets of monazite age data from 17 points measured on 16 monazite grains confirm the weighted average of 167±12 Ma. The obtained results confirm the age of the subduction/accretion processes related to the tectonothermal overprint of the Meliata accretionary wedge, in which fragments of the Southern Gemeric continental margin (slivers of the Bučina Formation) were also involved. Existence of the identical ages in monazite grains from the volcanites of the Southern Gemeric Unit documents the high intensity of the subduction-related fluid flows, which penetrated over the thinned Hercynian Southern Gemeric basement. The data obtained confirm the active continental margin tectonic setting of the Southern Gemeric crystalline basement and their Permian envelope during the Meliata subduction/accretion orogeny.

The weighted average age of 136±10 Ma reflects the successive Early Cretaceous compression. Polyphase Alpine tectonic evolution connected with the gradual Cretaceous collision and indentation also confirmed by the youngest age data set of 100±11 Ma.

Acknowledgments: The financial support of Scientific Grant Agency of the Ministry of Education of Slovak Republic and the Slovak Academy of Sciences (Project No. 1/1036/04) and Slovak Research and Development

Support Agency (Project ID: APVV-0438-06 and APVT 51-002804) is gratefully acknowledged. The authors would like to thank M.A. Kusiak, D. Plašienka and I. Petrík who constructively led to significant improvement of the manuscript.

References

Andrusov D. 1936: Subtatric Nappes in the Western Carpathians. *Carpatica* 1, 3–50 (in Slovak).

Andrusov D. 1968: Grundriss der Tektonik der Nördlichen Karpaten. *Slovak Acad. Sci*., Bratislava, 1–188.

Andrusov D., Bystrický J. & Fusán O. 1973: Outline of the structure of the West Carpathians — Guide-book for geol. excursion. *X. Congr. of CBGA*, Bratislava, *D. Štúr Inst. Geol*., Bratislava, 1–44.

Bajaník Š., Vozárová A. & Reichwalder P. 1981: Lithostratigrafic classification of Rakovec Group and Late Paleozoic in the Spišsko-gemerské rudohorie Mts. *Geol. Práce, Spr.,* Bratislava, 75, 27–56 (in Slovak).

Bajaník Š., Hanzel V., Ivanička J., Mello J., Pristaš J., Reichwalder P., Snopko L., Vozár J. & Vozárová A. 1983: Explanation to the geological map of the Slovenské rudohorie Mts., eastern part 1:50,000. Bajaník Š. & Vozárová A. (Eds.). *D. Štúr Inst. Geol*., Bratislava, 1–223 (in Slovak).

Bajaník Š., Ivanička J., Mello J., Pristaš J., Reichwalder P., Snopko L., Vozár J. & Vozárová A. 1984: Geological map of the Slovenské rudohorie Mts.-eastern part, 1:50,000. *D. Štúr Geol. Inst.*, Bratislava.

Broska I., Vozár J., Uher P. & Jakabská K. 1993: Zircon typology from the Permian rhyolite-dacites and their volcaniclastics (Western Carpathians). In: Rakús M. & Vozár J. (Eds.): Geodynamic evolution and deep structure of the Western Carpathians. *D. Štúr Geol. Inst.*, Bratislava, 151–158 (in Slovak).

Dallmeyer R.D., Neubauer F., Handler R., Fritz H., Mueller W., Pana D. & Putiš M. 1996: Tectonothermal evolution of the internal Alps and Carpathians: Evidence from $^{40}Ar/^{39}Ar$ mineral and whole-rock data. *Eclogae Geol. Helv*. 89, 203–227.

Faryad S.W. & Henjes-Kunst F. 1997: Petrological and K-Ar and Ar^{40}–Ar^{39} age constraints for the tectonothermal evolution of the high-pressure Meliata unit, Western Carpathians (Slovakia). *Tectonophysics* 280, 141–156.

Fusan O. 1959: Remarks to the Late Paleozoic of the Gemerides. *Geol. Práce, Zoš.* 55, *D. Štúr Geol. Inst*., Bratislava, 171–181 (in Slovak).

Hurai V., Urban M., Konečný P., Thomas R., Lexa O., Schulmann K. & Chovan M. 2006: Cretaceous age of quartz-stibnite veins near Čučma (Spišsko-gemerské rudohorie). *Miner. Slovaca* 38, 131–140 (in Slovak).

Konečný P., Siman P., Holický I., Janák M. & Kollárová V. 2004: Methodics of monazite dating using an electron microprobe. *Miner. Slovaca* 36, 225–235 (in Slovak).

Lexa O., Schulmann K. & Ježek J. 2003: Cretaceous collision and intendation in the West Carpathians: View based on structural analysis and numerical modelling. *Tectonics* 22, 6, 1066, doi: 10.1029./2002TC001472.

Maluski H., Rajlich P. & Matte P. 1993: $^{40}Ar/^{39}Ar$ dating of the Inner Carpathians Variscan basement and Alpine mylonitic overprinting. *Tectonophysics* 223, 313–337.

Marsina K. (Ed.), Bodiš D., Havrila M., Janák M., Káčer Š., Kohút M., Lexa J., Rapant S. & Vozárová A. 1999: Geochemical atlas of Slovak Republic. Part III: *Rocks. Geol. Surv. Slovak of Rep. Ministry of Environment of Slovak Rep*., Bratislava, 1–135.

Mello J., Elečko M., Pristaš J., Reichwalder P., Snopko L., Vass D. & Vozárová A. 1996: Geological map of the Slovak Karst 1:50,000. *Geol. Surv. Slovak Rep.*, Bratislava.

Mello J., Elečko M., Pristaš J., Reichwalder P., Snopko L., Vass D., Vozárová A., Gaál Ľ., Hanzel V., Hók J., Kováč P., Slavkay M. & Steiner A. 1997: Explanation to geological map of the Slovak Karst, 1:50,000. *Geol. Surv. Slovak Rep.*, Bratislava, 1–255.

Mello J., Reichwalder P. & Vozárová A. 1998: Bôrka Nappe: high-pressure relic from the subduction-accretion prism of the Meliata Ocean (Inner Western Carpathians, Slovakia). *Slovak Geol. Mag*. 4, 261–274.

Mock R., Sýkora M., Aubrecht R., Ožvoldová L., Kronome B., Reichwalder P. & Jablonský J. 1998: Petrology and stratigraphy of the Meliaticum near the Meliata and Jaklovce villages, Slovakia. *Slovak Geol. Mag*. 4, 223–260.

Montel J.M., Foret S., Veschambre M., Nicollet Ch. & Provost A. 1996: Electron microprobe dating of monazite. *Chem. Geol*. 131, 37–53.

Planderová E. 1980: New data on the age of the Rožňava–Železník Group. *Geol. Práce, Spr.* 74, *D. Štúr Geol. Inst*., Bratislava, 113–119 (in Slovak).

Plašienka D., Grecula P., Putiš M., Kováč M. & Hovorka D. 1997: Evolution and structure of the Western Carpathians: An overview. In: Grecula P., Hovorka D. & Putiš M. (Eds.): Geological evolution of the Western Carpathians. *Geocomplex*, Bratislava 1–24.

Reichwalder P. 1973: Geologische Verhältnisse des jüngere Paläozoikum im SÖ Teil des Zips-Gemerer Erzgebirge. *Zborn. Geol. Vied, Západ. Karpaty* 18, 99–140 (in Slovak, Germ. Res.).

Rojkovič I. & Konečný P. 2005: Th-U-Pb dating of monazite from the Cretaceous uranium vein mineralization in the Permian rocks of the Western Carpathians. *Geol. Carpathica* 56, 493–502.

Suzuki K. & Adachi M. 1991a: Precambrian provenance and Silurian metamorphism of the Tsubonosawa paragneiss in the South Kitakami terrane, Northeast Japan, revealed by the chemical Th-U-total Pb isochron ages of monazite, zircon and xenotime. *J. Geoch.* 25, 357–376.

Suzuki K. & Adachi M. 1991b: The chemical Th-U-total Pb isochron ages of zircon and monazite from the Gray Granite of the Hida Terrane, Japan. *J. Earth Sci., Nagoya Univ.* 38, 11–37.

Suzuki K. & Adachi M. 1994: Middle Precambrian detritalmonazite and zircon from Hida gneiss on Oki-Dogo Island, Japan: their origin and implications for correlation of basement gneiss of Southwest Japan and Korea. *Tectonophysics* 235, 277–292.

Šmelko M. 2007: Petrological and geochemical character of the Southern Gemericum and Bôrka Nappe acid volcanism with using of zircon as mineral indicator. *Master Thesis*, *Com. Univ. Fac. Nat. Sci.*, Bratislava, 1–66.

Šucha V. & Eberl D.D. 1992: Postsedimentary alteration of the Permian sediments in the northern Gemericum and Hronicum of the Western Carpathians. *Miner. Slovaca* 24, 399–405 (in Slovak).

Šuf J. 1963: Report on geological research in Štítnik. *Geol. Práce, Spr.*, Bratislava, 27, *D. Štúr Geol. Inst.* 63–68 (in Czech).

Vozárová A. 1996: Tectono-sedimentary evolution of Late Paleozoic Basins based on interpretation of lithostratigraphic data (Western Carpathians, Slovakia). *Slovak Geol. Mag.* 3–4, 251–271.

Vozárová A. & Rojkovič I. 2000: Permian lacustrine phosphatic sandstone in the Southern Gemeric unit, Western Carpathians, Slovakia. *Geol. Carpathica* 51, 265–278.

Vozárová A. & Vozár J. 1988: Late Palaeozoic in West Carpathians. *Monogr., D. Štúr Geol. Inst.*, Bratislava, 1–314.
Vozárová A. & Vozár J. 1996: Terranes of West Carpathian-North Pannonian Domain. *Slovak Geol. Mag.* 1, 61–83.
Vozárová A., Frank W. & Kráľ J. 2000: $^{40}Ar/^{39}Ar$ data from contact aureole of Súľová granite (Gemericum, Western Carpathians). *Slovak Geol. Mag*. 4, 363–366.
Vozárová A., Frank W., Kráľ J. & Vozár J. 2005: $^{40}Ar/^{39}Ar$ dating of detrital mica from the Upper Paleozoic sandstones in the Western Carpathians. *Geol. Carpathica* 56, 463–472.